Diagnosis of Faults in Rolling Element Bearings by Using Directional Spectra of Vibration Signals

Jong-Po Park* and Chong-Won Lee**

(*Received June 20, 1998*)

Backward and forward defect frequencies of rolling element bearings are experimentally investigated utilizing the two-sided directional spectra of the complex-valued vibration signals measured from the outer ring of defective bearings. The experimental results show that the directional zoom spectrum is superior to the conventional spectrum in identification of bearing defect frequencies, in particular the inner race defect frequencies.

Key Words: Rolling Element Bearing, Fault Diagnosis, Defect Frequency, Maximum Likelihood Spectrum, Directional Spectrum

1. Introduction

Many techniques, which analyze vibration signals to detect faults in rolling element bearings, are available. These techniques include shock pulse monitoring, crest factor analysis, kurtosis, spectrum analysis and envelope power spectral density (PSD) analysis (Bell, 1985; McFadden and Smith, 1984; White, 1991). Due to the fact that bearing faults often produce low level vibrations which are likely to be masked by vibrations from other components such as gears and shafts, the envelope PSD analysis, or also known as the demodulated resonance analysis, has gained much attention, and has found to be a useful method to detect the defect frequency. However, since this method utilizes the spectrum indirectly, it does not exploit all the information contained in the spectrum (Sherman and Lou, 1989). Note that this information includes not only the bearing defect frequency, but also the valuable *directivity, backward and forward*, associated with rotating defects (Lee, 1993).

In recent years, the *directional* power spectrum (dPS) of complex-valued vibration signals has been proven to be a powerful diagnostic tool for rotating machinery (Lee, 1993; Lee and Joh, 1994; Joh and Lee, 1996). The key idea is that, in general, a planar whirling motion of a rotor in operation can be decomposed into *backward* (the direction opposite to the rotor rotation) and *forward* (the same direction as the rotor rotation) harmonic components. The harmonic components, backward or forward, can be directly identified in the directional spectrum. Thus the variations in forward and backward frequency components of the dPS can be effectively used for diagnosing any defects or faults in a rotating machine. The dPS technique, originally developed for rotating machinery, has been proved to be effective for nonrotating machines as well (Lee et al., 1995 and 1997, Park et al., 1998). On the other hand, as a spectral estimator, the FFT method has inherent limitations related to frequency resolution, variability, and inability to discern between narrow-band random and true periodic components, while Maximum Likelihood (ML) spectral estimators possess better capabilities in power estimation (Sherman and Lou, 1989; Kay, 1988; Shernam, 1991). The *directional* ML spectral estimator (Lee et al., 1995 and 1997) is introduced to account for *complex*-valued signals and utilized as a comple-

* Research and Development Center Korea Heavy Industries & Construction Co., Ltd. 555 Guygok-Dong, Changwon 641-792 KOREA

** Center for Noise and Vibration Control (NOVIC) Department of Mechanical Engineering Korea Advanced Institute of Science and Technology Science Town, Taejon 305-701 KOREA

ment to the FFT estimator in this work.

In this paper, backward and forward defect frequencies of ball bearings are experimentally investigated utilizing the dPS of the complex-valued vibration signals measured from the outer ring of ball bearings with artificial defects in inner and outer races. Effectiveness of the dPS for the diagnosis and frequency identification of bearing defects is experimentally demonstrated, compared with the conventional power spectrum method.

2. Bearing Defect Frequency

Let us consider a defective ball bearing, as shown in Fig. 1, of which the inner race rotates at a constant speed Ω and the stationary outer race is subjected to a constant axial load. Each time a defect in a bearing surface comes into contact with another surface, an impact type force is generated, resulting in an impulsive response of the bearing. Because the contacts between the defect and the mating surfaces in the bearing are essentially periodic, the impulse will recur at regular intervals; the frequency of occurrence of the impulse is referred to as the characteristic defect frequency, which depends on the location of the defect. Among others, the ball pass frequencies, f_i and f_o, for an inner race and outer race defect, which are often abbreviated as BPFI and BPFO, respectively, are given as (Bell, 1985)

$$f_i = n(\Omega - f_c) = \frac{n\Omega}{2}\left[1 + \frac{d}{D}\cos\alpha\right] \tag{1}$$

$$f_o = nf_c = \frac{n\Omega}{2}\left[1 - \frac{d}{D}\cos\alpha\right] \tag{2}$$

where f_c is the fundamental train frequency (FTF) given by

$$f_c = \frac{\Omega}{2}\left[1 - \frac{d}{D}\cos\alpha\right] \tag{3}$$

In the above expressions, d and D are the ball and the pitch circle diameters, n is the number of balls, and α is the contact angle. Note here that BPFI and BPFO are defined with respect to the coordinate frame fixed to the defective race.

It will prove convenient to introduce two coordinate systems, as shown in Fig. 1, for the defect signal analysis: one is the stationary coordinate system, xyz, and the other is the rotating coordinate system, $x\xi\eta$, which is fixed to the inner race and spins relative to the stationary coordinate system at the rotational speed Ω. The complex-valued signals can then be defined in the stationary coordinate system as

$$p(t) = y(t) + jz(t) \tag{4}$$

or equivalently in the rotating coordinate system as

$$q(t) = \xi(t) + j\eta(t) \tag{5}$$

where y and z (ξ and η) are the vibration signals measured in the y and z (ξ and η) directions with respect to the stationary (rotating) coordinate system, and j denotes the unit imaginary number. The relationship between the complex signals in two coordinate systems are given by

$$p(t) = q(t)\exp(j\Omega t) \tag{6}$$

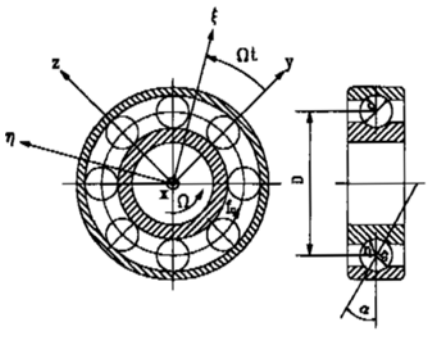

Specifications of Test Bearings	
Bearing Type	6204
Number of Balls (n)	8
Contact Angle(α)	13.0°
Ball Diameter(d)	7.938 mm
Pitch Circle Diameter(D)	34.50 mm
Groove Radius of Inner Ring(r_i)	4.01 mm
Groove Radius of Outer Ring(r_o)	4.20 mm
Cage Material: Polyamid Plastic Shaft Rotating Speed(Ω): 40 rps	

Units: mm

Specifications of Bearing Defects			
Location	Depth	Width	Machining
Inner Race	0.1	1.0	Electro-Discharging
Outer Race	0.1	1.0	Electro-Discharging

Fig. 1 Coordinate systems and specifications of test bearings.

It should be noted that the periodic impulsive force induced by an inner race defect also rotates with the shaft at the frequency $+\Omega$ unlike the impulsive force due to an outer race defect. When the observation is made in the stationary coordinate system, the vibration signal from the bearing due to an inner race defect can be approximated as

$$\begin{aligned} p_i(t) &= q_i(t)\exp(j\Omega t) \\ &= \sum_{k=1}^{\infty}[q_k^b \exp\{-j(kf_i-\Omega)t\} \\ &\quad + q_k^f \exp\{j(kf_i+\Omega)t\}] \end{aligned} \tag{7}$$

where $q_i(t)$ denotes the complex vibration signal measured in the rotating coordinate system, which is caused by an inner race defect, and the superscripts b and f denote the backward and forward components, respectively. Since the outer race is stationary, the vibration signal from the bearing due to an outer race defect can be approximated as

$$p_o(t) = \sum_{k=1}^{\infty}[p_k^b \exp(-jkf_o t) + p_k^f \exp(jkf_o t)] \tag{8}$$

The presence of higher-harmonic components in Eqs. (7) and (8) is attributed to the periodic impulsive response induced by the defect. Equation (7) indicates that the difference in magnitude between the backward and forward defect frequencies is 2Ω. Fourier-transforming Eq. (7), we obtain

$$P_i(f) = Q_i(f-\Omega) \tag{9}$$

where $P_i(f)$ and $Q_i(f)$ are the Fourier transforms of $p_i(t)$ and $q_i(t)$, respectively, and f means the frequency. Equation (9) indicates that the response spectrum due to an inner race defect is shifted by an amount of $+\Omega$ due to the coordinate transformation from the rotating to the stationary coordinate system.

The dPS of the complex-valued signal $p(t)$ defined in Eq. (4) is given as (Lee et al., 1995 and 1997)

$$P_{pp}(f) = P_{yy}(f) + P_{zz}(f) + j(P_{yz}(f) - P_{zy}(f)) \tag{10}$$

where, $P_{ik}(f)$, i, k=p, y, z, are the power spectra. Each dPS will have non-negative real values at some discrete frequencies for finite duration deterministic signals but they become continuous functions of the frequency f for random signals. Note that the dPS defined in Eq. (10) gives not only frequency content but also directivity and shape of the motion on the y-z plane, unlike the conventional PS which only gives one-sided frequency content. In this way, the dPS contains richer information regarding the planar motion than the PS.

3. Experimental Set-up

Figure 2 shows the experimental set-up for diagnosis of the ball bearing defect. The geometry

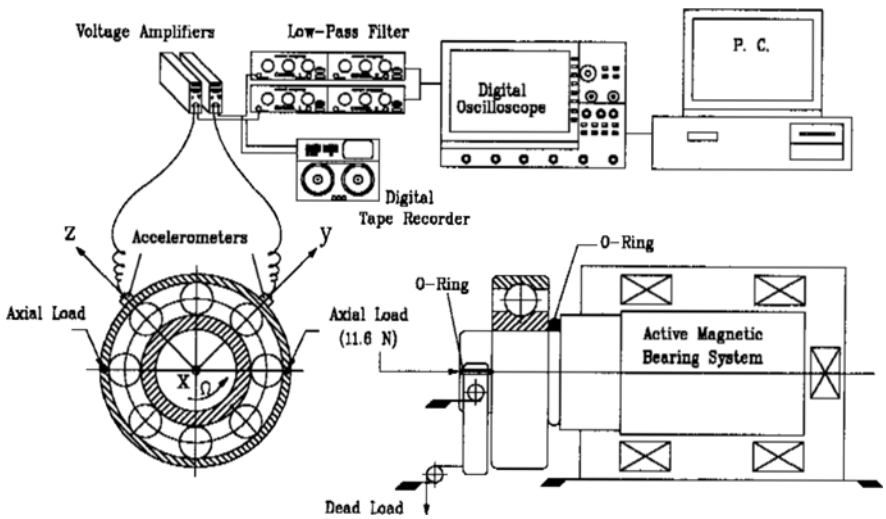

Fig. 2 Schematic diagram of experimental set-up for ball bearing diagnosis.

and defect specifications of test bearings are given in Fig. 1, in which the length of inner (outer) race defect is equal to that of inner (outer) race groove. A laboratory 5-axis active magnetic bearing system with less than 2 μm radial vibration was employed as the driving spindle for precision operation. Throughout the experiments, the rotational speed of the spindle was kept to be 40 rps. To prevent a slip of balls in the bearing, a constant axial load of 11.6 N was applied to the outer ring of the test bearing by using a dead weight type preloader, and mineral oil instead of grease was used as the lubricant during the experiments. The contact angle α was calculated to be 13° under such load condition. The resulting y -and z-directional vibrations were sensed by two transducers mounted perpendicular to each other on the free exterior of the outer ring. The transducers are piezoelectric accelerometers which have good response characteristics over high frequency range. The output voltages from amplifiers were recorded in a digital tape recorder. The playback signals were filtered using antialiasing analog filters with the cutoff frequency of 6kHz and monitored before they were subsequently sampled at a rate of 20 kHz by a four channel digital oscilloscope, and analysed by a 32-bit personal computer.

Preliminary impact tests were performed to check the natural modes associated with the outer ring where the two accelerometers are mounted. The tests results showed that there existed a strong ring mode at 4.15 kHz.

4. Results and Discussions

The characteristic defect frequencies of test bearings were calculated by using Eqs. (1) and (2) for the rotational speed of 40 rps and the contact angle of 13°, prior to the measurements, i. e.

BPFI, $f_i = 195.9$ Hz $\cong 4.9X$

BPFO, $f_o = 124.1$ Hz $\cong 3.1X$

where X denotes the rotational speed of the inner race. When observations are made in the stationary coordinate, the backward and forward defect frequencies for an inner race defect can be calculated as $-3.9X$ and $+5.9X$, respectively, using Eqs. (7) and (9). In this section, we discuss four different methods to identify the bearing defect frequencies from the measured vibration signals: waveform analysis, baseband spectrum analysis, envelope spectrum analysis and zoom spectrum analysis.

4.1 Waveforms of vibration due to defects

Figure 3 shows the acceleration signals measured from test bearings, which were low-pass filtered at 6 kHz cutoff frequency and subsequently sampled at 20 kHz. As each ball passes over the

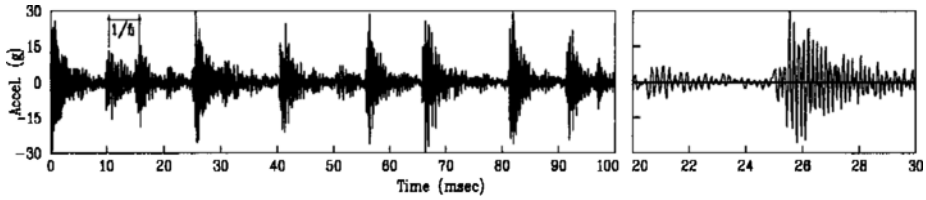

(a) Inner race defect

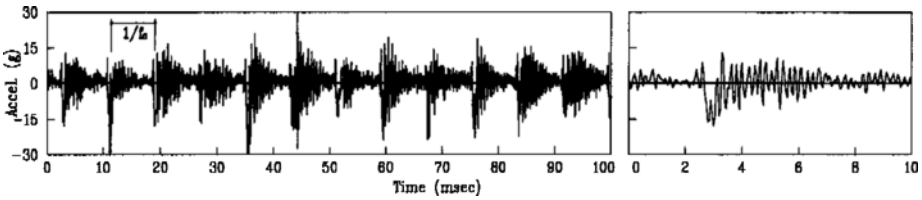

(b) Outer race defect

Fig. 3 Acceleration signals from defective bearings.

defect, a very sharp impulse is generated, which in turn excites the outer ring resonant modes, in particular the fundamental mode. It gives rise to a series of short trains of damped vibrations at the resonant frequency (Mcfadden and Smith, 1984; White, 1991). In other words, the end result consists of periodic bursts of exponentially decaying sinusoidal vibration. The frequency and decay rate of the vibration are associated with the natural frequency and internal damping of the outer ring. For the inner race defect in Fig. 3(a), it is not straightforward to find the two characteristic defect frequencies in the signal: -3.9X and $+5.9$X. Even the period associated with ± 4.9X is not clearly recognized. It is due to the fact that the inner race defect frequency of ± 4.9X in the rotating coordinate system is amplitude modulated by the rotational speed $+\Omega$, resulting from the coordinate transformation, as seen in Eqs. (6) and (7). Figure A-1 in Appendix clearly supports the above observation. On the other hand, we can easily observe the periodic impulse response associated with the outer race defect frequency of ± 3.1X as shown in Fig. 3(b).

4.2 Baseband spectra

Figures 4(a) and 5(a) show the typical baseband dPSDs of the vibration signals taken from the bearing with an inner race defect. The weak 3.1X components shown in Fig. 5(a) and (b) are attributed to machining-inherited imperfect roundness in the outer race of normal bearings. The characteristic defect frequency is not clearly identified in the dPSDs, unlike the harmonics of rotational speed, resulting from the amplitude modulation of the outer ring resonant frequency by the defect signal as shown in Figs. 3 (a) and 4(a). It should also be noted that almost all spectral energy is distributed near the resonant frequency, along with strong sideband families. On the other hand, for an outer race defect, the characteristic defect frequency and its higher-harmonic contents are clearly observed as shown in Figs. 4(b) and 5(b). Figure 4(b) shows that almost all spectral energy is concentrated into the defect frequency and its harmonics and that some energy is also distributed at the resonant frequency and its sideband. The significant difference in degree of the amplitude modulation between two cases is attributed to the different passage between each excitation source and the

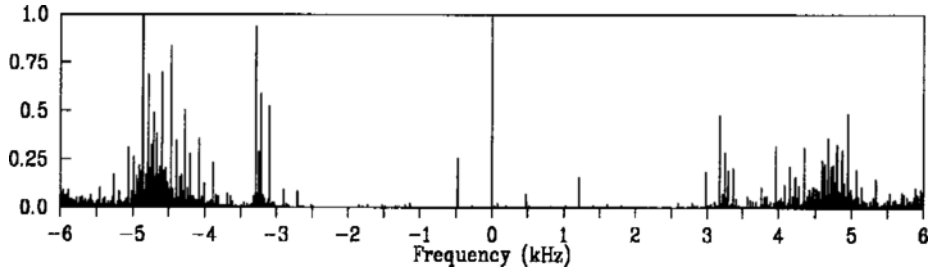

(a) Inner race defect

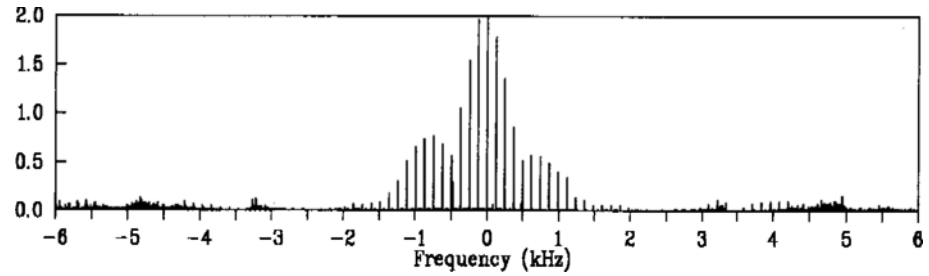

(b) Outer race defect

Fig. 4 Typical baseband dPSDs of vibration signals from defective bearings.

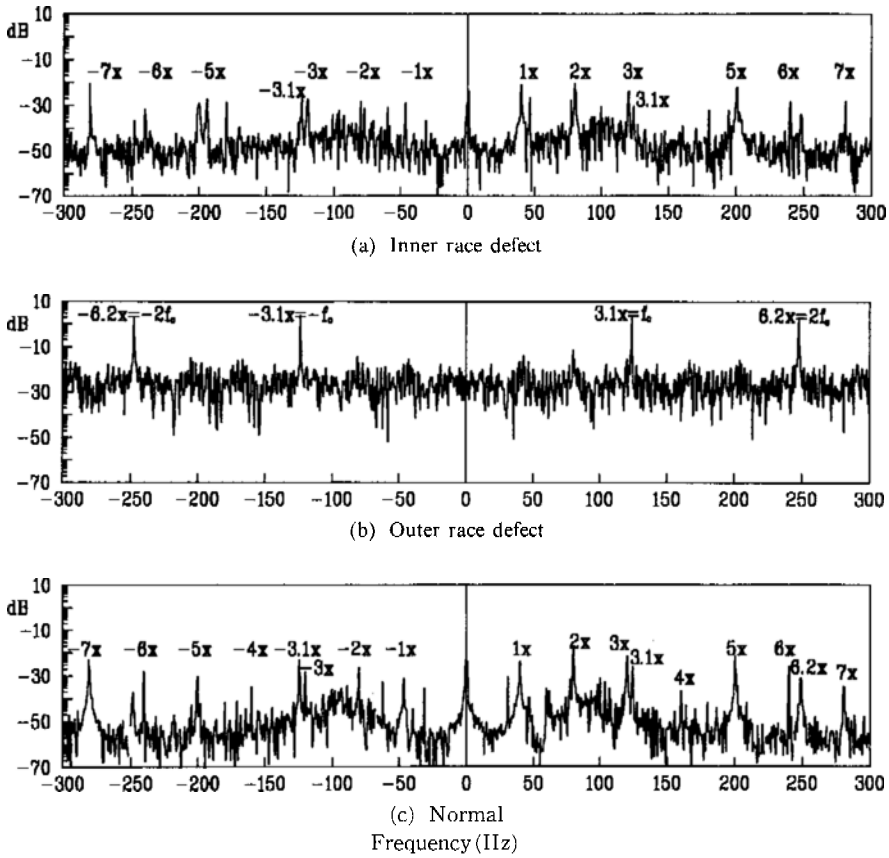

Fig. 5 dPSDs of vibration signals from test bearings.

response measurement locations: one takes a direct path but the other takes an indirect one.

4.3 Envelope spectra

To detect the repetition rate of energy burst in amplitude modulated signals, the amplitude demodulation technique is commonly adopted to obtain the signal envelope (Bell, 1985; Randall, 1987). Figure 6 shows the PSDs of the resulting vibration signal envelopes, where the dPSD was acquired from the FFT of the complex envelopes of which real and imaginary parts were made up with the y- and z-directional envelopes, respectively. Since the envelope itself loses the directivity information which has persistently been present in the original burst signals, the frequency shift by an amount of $+\Omega$ and the defect frequencies, -3.9X and $+5.9$X, for an inner race defect, are not observed. Figure A-2 in Appendix also supports the above observation.

4.4 Zoom spectra

A zoom frequency analysis centered at the outer ring resonance of 4.15 kHz, as an alternative to the previous techniques, was made to investigate the backward and forward defect frequencies. To calculate the zoom dPS, the sampled 32768 complex datapoints were digitally filtered in the frequency band between 3.65 kHz and 4.65 kHz, modulated by a 3.5 kHz cosine wave, and then low-pass filtered at 1.15 kHz. Finally, the filter output was resampled at 5 kHz, resulting in 8192 complex datapoints. Note that the reduced resampling rate of 5 kHz allows a rapid convergence of ML spectra to signal spectra, as the model order increases (Sherman and Lou, 1989; Lee et al., 1995 and 1997).

The zoom spectra are shown in Fig. 7, in which the sideband peaks, equally-spaced by the characteristic defect frequencies, around the carrier frequency are clearly observed as expected. The

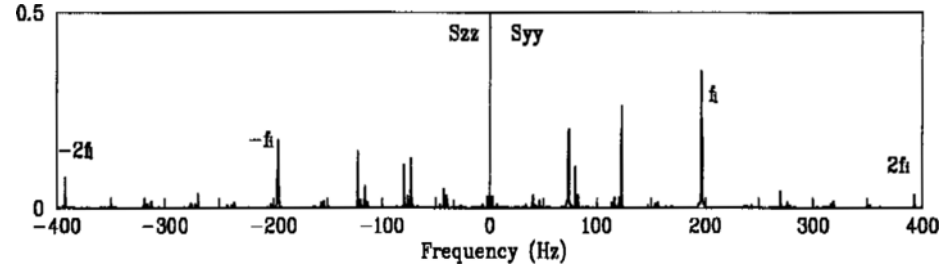

(a) Conventional

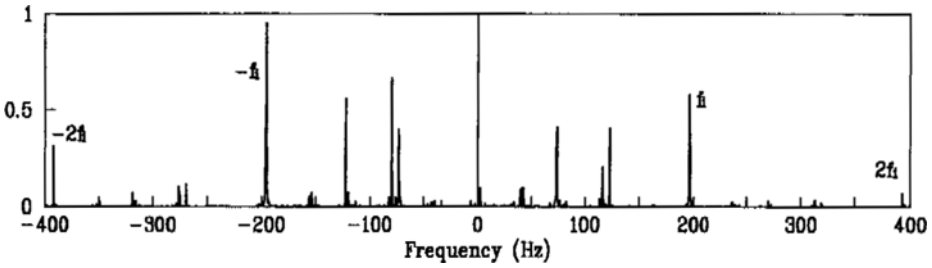

(b) Directional

Fig. 6 Envelope PSDs of vibration signal from a bearing with an inner race defect.

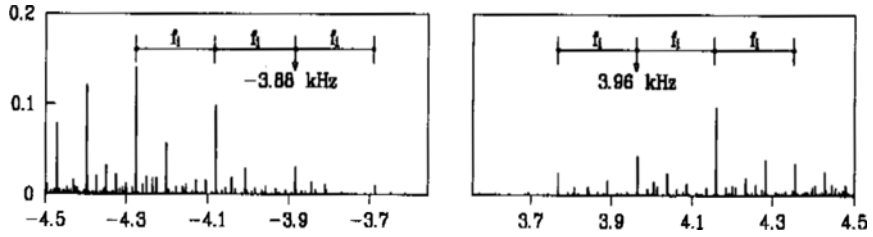

(a) Inner race defect

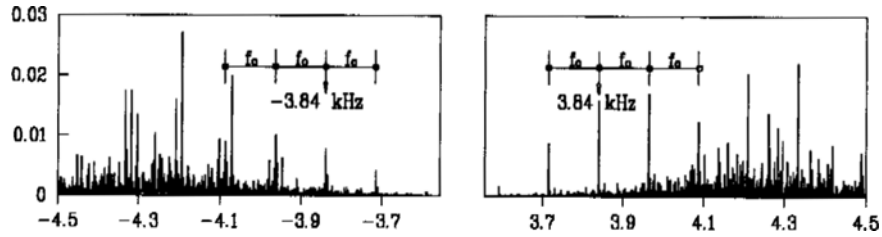

(b) Outer race defect

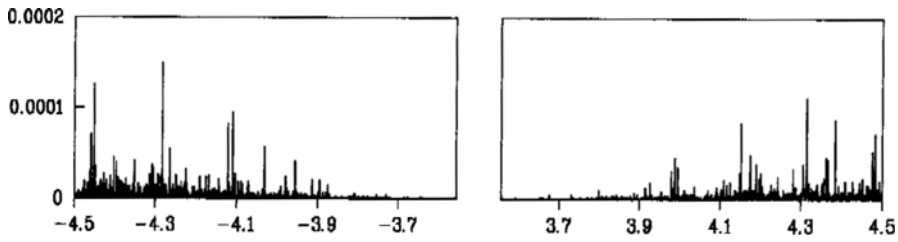

(c) Normal

Frequency (kHz)

Fig. 7 Zoomed dPSDs of vibration signals from test bearings.

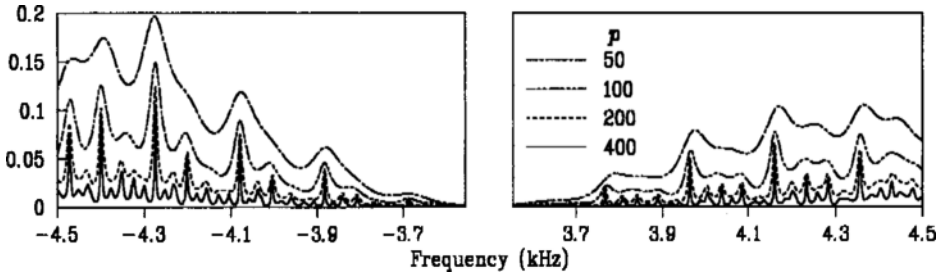

Fig. 8 Zoomed ML dPSs of vibration signals from a bearing with an inner race defect.

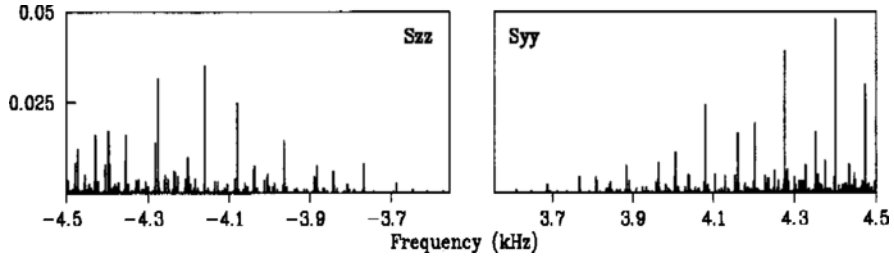

(a) Inner race defect

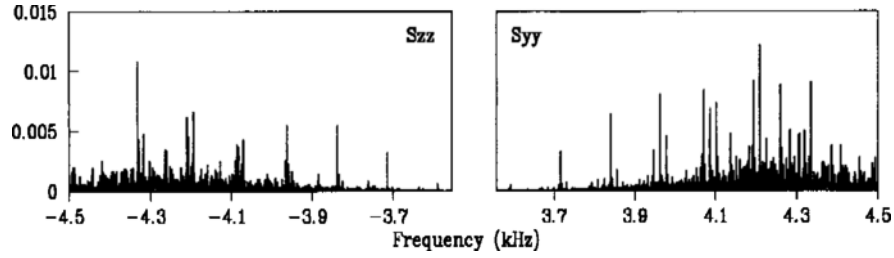

(b) Outer race defect

Fig. 9 Conventional PSDs of vibration signals from defective bearings.

multiple sideband peaks imply that the response, $p(t)$, to bearing defect before modulation is not of a pure harmonic but a periodic signal with the period equal to the inverse of the defect frequency. The modulated time signal, $r_i(t)$ ($r_o(t)$), for the inner (outer) race defect can be expressed, multiplying the defect time signal in Eq. (7) ((8)) by the carrier signal, as

$$r_i(t) = p_i(t)\,[A_i^b \exp(-j\omega_i t) + A_i^f \exp(j\omega_i t)] \quad (11)$$

or

$$r_o(t) = p_o(t)\,[A_o^b \exp(-j\omega_o t) + A_o^f \exp(j\omega_o t)] \quad (12)$$

where the subscript i (o) denotes the inner (outer) race defect, and ω_i (ω_o) is the outer ring resonant or carrier frequency for the inner (outer) race defect case. Figure 8 shows the typical ML dPS for an inner race defect, where the monotonic convergence of the defect or modulating frequency is clearly observed as model order p increases (Sherman and Lou, 1989; Lee et al., 1995 and 1997), which were obscured in the dPSD estimated by the FFT as shown in Fig. 7 (a). Note that we can not only detect the well-separated backward and forward components of the characteristic defect frequency, but also observe the frequency shift by an amount of $+\Omega$ in the directional spectra for the inner race defect case. This observation verifies the fact that the backward and forward defect frequencies for an inner race defect is $-f_i+\Omega$ and $f_i+\Omega$, respectively. Figure A-3 in Appendix also supports the above observation.

A comparison between the directional and the conventional zoom spectra, as shown in Figs. 7

and 9, indicates that the conventional spectra result in folding of the forward and backward frequency components in one-sided frequency region, unlike the directional spectra. Thus, it is rather difficult, if not impossible, to find the defect frequencies and the frequency shift from the conventional spectra for inner race defect. For this reason, it is believed that experimental studies using the conventional spectra in the past have failed to find the rotating defect frequencies corresponding to inner race defects.

In conclusion, the zoom analysis of dPS centered at the outer ring resonance can be effectively used to identify the bearing defect frequencies.

5. Conclusions

A zoom technique with the dPS centered at the stationary ring resonance is developed for identification of bearing defect frequencies. Experimental results show that the proposed technique successfully identifies bearing defect frequencies, in particular the backward and forward frequencies associated with rotating defect.

References

Bell, D. H., 1985, "An Enveloping Technique for Early Stage Detection and Diagnosis of Faults in Rolling Element Bearings," *Proc. 10th ASME Biennial Conf. on Mechanical Vibration and Noise*, pp. 65~69.

Joh, C. Y. and Lee, C. W., 1996, "Use of dFRFs for Diagnosis of Asymmetric/Anisotropic Properties in Rotor-Bearing System," *ASME J. Vibration and Acoustics*, Vol. 117, pp. 64~69.

Kay, S. M., 1988, *Modern Spectral Estimation*, Prentice-Hall.

Lee, C. W., 1993, *Vibration Analysis of Rotors*, Kluwer Academic Publishers.

Lee, C. W., Han, Y. S., and Park, J. P., 1997, "Use of Directional Spectra for Detection of Engine Cylinder Power Fault," *Shock and Vibration*, Vol. 4(5), pp. 391~401

Lee, C. W. and Joh, C. Y, 1994, "Use of Directional Spectra for Diagnosis of Asymmetry/Anisotropy in Rotor Systems," *Proc. 4th Int. Conf. on Rotor Dynamics*, Chicago, USA, pp. 97~101.

Lee, C. W., Park, J. P., and Han, Y. S., 1995, "Use of Directional AR and ML Spectra for Detection of Misfired Engine Cylinder," *Proc. 15th ASME Biennial Conf. on Vibration and Noise* 3(A), Boston, USA, pp. 1397~1403.

McFadden, J. M. and Smith, J. D., 1984, "Vibration Monitoring of Rolling Element Bearings by the High-Frequency Resonance Technique-a Review," *Tribology International*, Vol. 17(1), pp. 3~10.

Park, J. P., Han, Y. S., and Lee, C. W., 1998, "Detection of Engine Cylinder Power Fault Using Directional AR and ML Spectra," submitted to KSME for possible publication.

Randall, R. B., 1987, *Frequency Analysis*, B & K Co. Ltd., 3rd ed.

Sherman, P. J., 1991, "Three Techniques for Harmonic Retrieval in Unknown Colored Noise," *Mechanical Systems and Signal Processing*, Vol. 5(3), pp. 183~197.

Sherman, P. J. and Lou, K. N., 1989, "Application of the ML Spectral Estimates for Identification of Defects in Rotating Machinery," *Proc. 7th Int. Conf. on Modal Analysis*, Las Vegas, USA, pp. 1587~1590.

White, G., 1991, "Amplitude Demodulation-A New Tool for Preventive Maintenance," *Sound and Vibration*, Vol. 25(9), pp. 16~19.

Appendix

Spectra of Amplitude Modulated Singal

Waveform and spectrum of an amplitude modulated signal are numerically investigated to support the analysis of the experimental data used in this work. The amplitude modulated signal is defined as

$$r(t) = q(t)\,u(t)\,v(t) \qquad (A\text{-}1)$$

where

$$q(t) = \sum_{k=1}^{K} [\exp(-jkf_i t) + \exp(jkf_i t)] + 1$$

$$u(t) = \exp(j\Omega t)$$

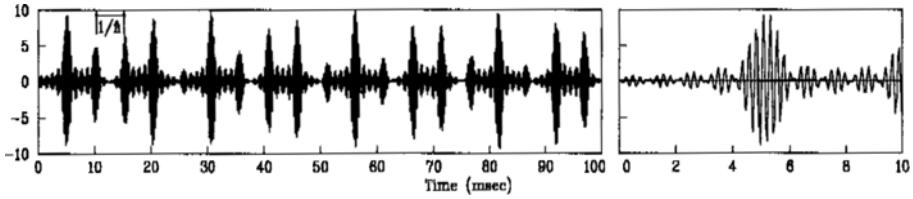

A-1 Waveform of amplitude modulated signal.

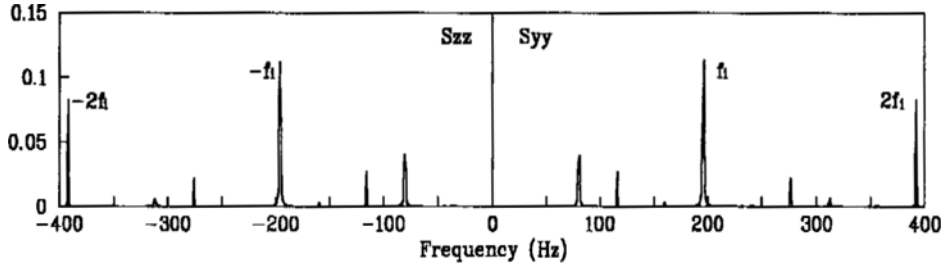

(a) Conventional

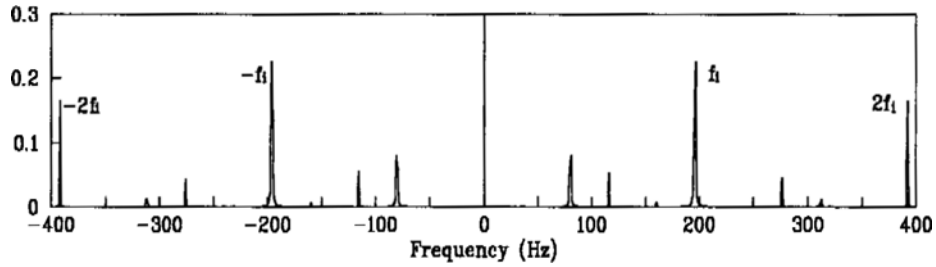

(b) Directional

A-2 Envelope PSDs of amplitude modulated signals.

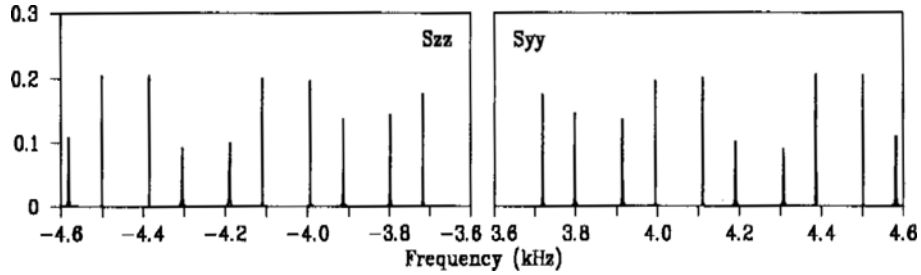

(a) Conventional

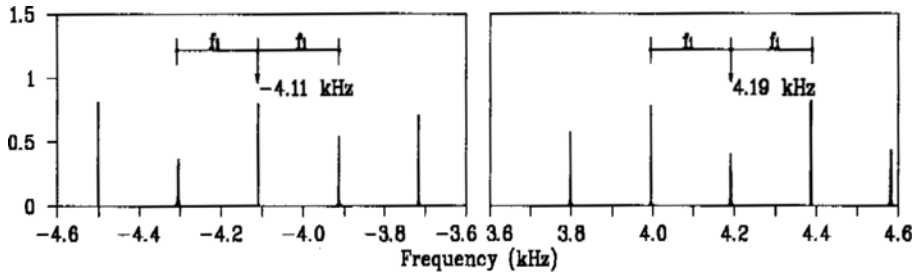

(b) Directional

A-3 PSDs of amplitude modulated signals.

$$v(t) = \exp(-j\omega t) + \exp(j\omega t)$$

Here, the complex vibration signal $q(t)$, $u(t)$, and $v(t)$ are associated with the frequency contents, observed in the rotating coordinate system, of the inner race defect, the coordinate transformation from the rotating to the stationary coordinate systems, and the outer ring resonance, respectively. The signal $r(t)$ is generated with $f_i = 2\pi \times 196$ rad/sec, $K = 2$, $\Omega = 2\pi \times 40$ rad/sec, and $\omega = 2\pi \times 4150$ rad/sec. Figures A-1, A-2 and A-3 show the waveform, envelope and baseband PSDs of the resulting vibration signal, respectively.